Title

Electronic structure and photovoltaic application of BiI3

Journal

Applied Physics Letters, 107(13)

ISSN

0003-6951 1077-3118

Authors

Lehner, Anna J

Wang, Hengbin

Fabini, Douglas H

et al.

Publication Date

2015-09-28

DOI

10.1063/1.4932129

Peer reviewed

Electronic structure and photovoltaic application of BiI_3

Anna J. Lehner,[1,2,a)] Hengbin Wang,[1] Douglas H. Fabini,[2,3] Christopher D. Liman,[1,3] Claire-Alice Hébert,[2] Erin E. Perry,[1,3] Ming Wang,[1,4] Guillermo C. Bazan,[1,3,4] Michael L. Chabinyc,[1,3] and Ram Seshadri[1,2,3,4]
[1)]*Mitsubishi Chemical Center for Advanced Materials, University of California, Santa Barbara, CA 93106*
[2)]*Materials Research Laboratory, University of California, Santa Barbara, CA 93106*
[3)]*Materials Department, University of California, Santa Barbara, CA 93106*
[4)]*Department of Chemistry and Biochemistry, University of California, Santa Barbara, CA 93106*

(Dated: 15 September 2015)

Rapid recent improvement in photovoltaic efficiency in hybrid lead halide perovskite materials has provided the impetus for understanding other, related main-group halide systems. Here we show that the closely related but less toxic bismuth iodide BiI_3 can show promising optoelectronic properties. Layered binary BiI_3 is used here as the active layer in planar solar cell architectures (efficiency approximately 0.3%). Experimental and computation studies of absolute band positions of BiI_3 are also presented, to help in the rational design of device architectures that would allow efficient charge transfer at the interfaces.

Keywords: Ultraviolet Photoelectron Spectroscopy, Density Functional Theory, Photovoltaic Devices

Bismuth triiodide BiI_3 belongs to a family of layered heavy metal semiconductors with interesting anisotropic electronic and optical properties.[1,2] Thin films and single crystals of BiI_3 have been investigated as hard radiation detectors[3–6] and for X-ray imaging[7–9] due to the relatively wide band gap, high atomic numbers of the constituent elements, and high mass density. Additionally, BiI_3 can be solution-processed, which could facilitate large-scale, cost-efficient and flexible device fabrication. However, there appear to be few attempts to use BiI_3 in photovoltaic devices. The prior report of BiI_3 described its use as hole transport layer (HTL) in solar cells with a fullerene-based light absorber.[10] Clearly the potential of bismuth halides as photovoltaic absorbers and less toxic alternatives to the prominent hybrid lead halide perovskites[11] has not been fully explored.[12]

The crystal structure of BiI_3 (space group $R\bar{3}$)[13] can be described as a slightly distorted hexagonally close packed lattice of I^- ions in which the metal cations occupy 2/3 of the octahedral voids of every other layer. Optical properties of BiI_3 have been extensively investigated.[14–19] The band gap (E_g) values reported for BiI_3 span a large range and the nature of the transition has caused some discussion. It has been suggested that the strong absorption at temperatures above 77 K (E_g approx. 1.8 eV, see Figure 1a) can be interpreted as a direct transition, while at lower temperature the lowest energy transition has been attributed to an indirect transition.[14,15,19] More recently, the transition at room temperature has been assigned to an indirect gap by optical absorption spectroscopy.[20]

Density functional theory (DFT) has been previously used to elucidate the electronic band structure of BiI_3 and confirm the indirect nature of the transition,[20,21] but only few recent studies[5,20–22] apply spin orbit coupling, which is necessary in 6s systems.[16,17] Most of those studies have been limited by the choice of using DFT within the local density approximation (LDA) or the generalized gradient approximation (GGA), which are known for poorly reproducing the band gaps of semiconductors. For photovoltaic applications, the knowledge of the absolute band positions is crucial for rational device design.

Here we present a study of the application of a bismuth halide as a photovoltaic absorber (active layer). To understand the properties of BiI_3 in photovoltaics, we examined its optical absorption and position of its electronic levels and compared them to other metal halide semiconductors relevant for solar cells. The absolute band positions of BiI_3 are determined experimentally by optical (UV-Vis) absorption and ultraviolet photoelectron spectroscopy (UPS) and computationally by a super-cell method[23] which is also valuable for related complex lead halides.[24] We have used the screened hybrid functional of Heyd, Scuseria, and Ernzerhof (HSE)[25] to obtain reliable values. Additionally, the dielectric response including the dielectric tensors (ϵ^∞) and the Born effective charge tensors (Z^*) of BiI_3 are presented as indicators of incipient structural instability and dielectric defect screening. BiI_3 solar cells were fabricated with a dense TiO_2 electron transport layer (ETL) and two different polymer HTLs.

The optical band gap of BiI_3 was determined by UV-Vis transmission spectroscopy of a film and diffuse reflection spectroscopy of a powder sample (Figure 1a, for details see supplemental material[26]). From both measurement modes, the band gap was determined to be approximately 1.8 eV assuming an indirect gap, which is well within the range of values reported previously.[20] The band structure presented in the following illustrates that the direct and indirect transition lie very close together. The ionization energy (I), which is the position of the valence band maximum (VBM) with respect to the vacuum energy, was determined experimentally from UPS (Fig-

[a)]Electronic mail: alehner@mrl.ucsb.edu

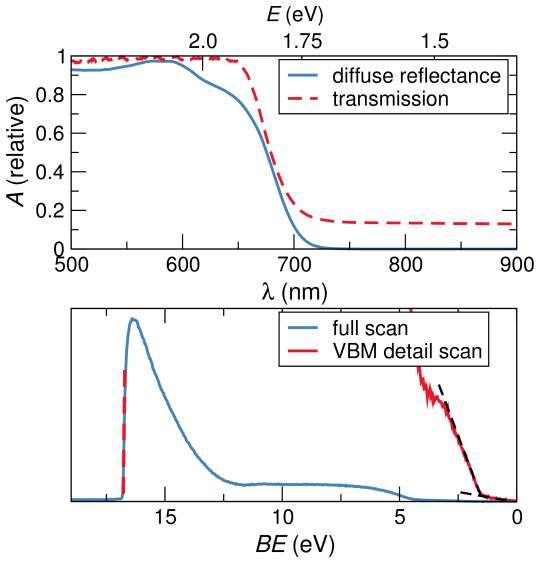

FIG. 1. (a) Diffuse reflectance (Kubelka-Munk transformed Absorbance A) and transmission (approx. 300 μm film thickness) UV-Vis and (b) UPS spectrum of BiI_3. From the UPS data, the position of the valence band maximum (VBM) was determined by subtracting the energy difference between both edges of the spectral feature from the excitation energy ($h\nu$ = 21.22 eV).

TABLE I. Experimental and calculated band gap (E_g) and ionization energy (I), calculated dielectric tensors (ϵ^{∞}_{ij}) and Born effective charge tensors (Z^*; $|e|$ on Bi^{3+}) of BiI_3.

E_g (eV)		I (eV)		ϵ^{∞}_{xx}	ϵ^{∞}_{zz}	Z^*_{xx}	Z^*_{zz}
exp.	calc.	exp.	calc.				
1.8	1.93	6.0 to 6.3	6.05	18.9	15.0	6.6	4.9

ure 1b) to lie between 6.0 and 6.3 eV for a range of measurements and samples (Table I). Spectra were collected on thin film samples whose surface composition was confirmed by X-ray photoelectron spectroscopy (XPS, for details see supplemental material[26]). This VBM level range is in good agreement with the value for the photoelectric work function of 5.8 eV reported previously.[17]

To support the experiments, DFT calculations of the band structures, band gaps, and absolute band positions were carried out using the VASP Package.[27,28] Spin-orbit-coupling (SOC) was included for all calculations. The input structure[13] was used without a structural relaxation step as the agreement between initial and optimized structure was poor due to inadequate description of the interlayer van der Waals interactions with the chosen method (see supplemental material[26]).

In order to compare the calculated electronic structure of BiI_3 to other phases, the VBM was normalized by the average electrostatic potential (Φ_{el}) obtained from slab calculations. Thereby, the ionization energy (I) was calculated following $I = \Phi_{el} - E_F$, where Φ_{el} is the difference between the potential energy of the empty (approximating the vacuum) and filled (approximating the

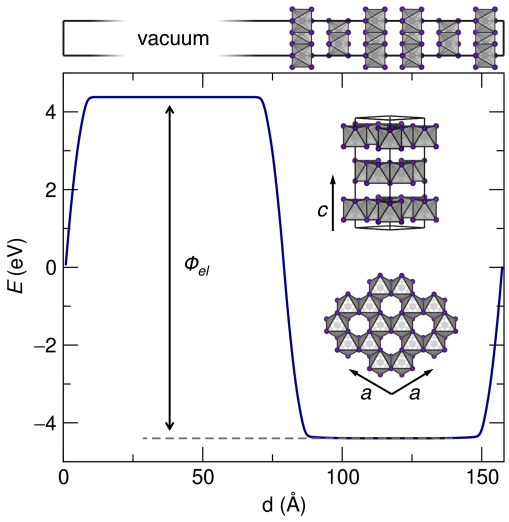

FIG. 2. Absolute band position calculation (DFT method PBE+SOC) for BiI_3 ($R\bar{3}$, see insets) using a slab model with a half filled 1×1×4 super-cell (model shown at top). Φ_{el} is the difference between the vacuum energy and the average electrostatic potential of the crystal.

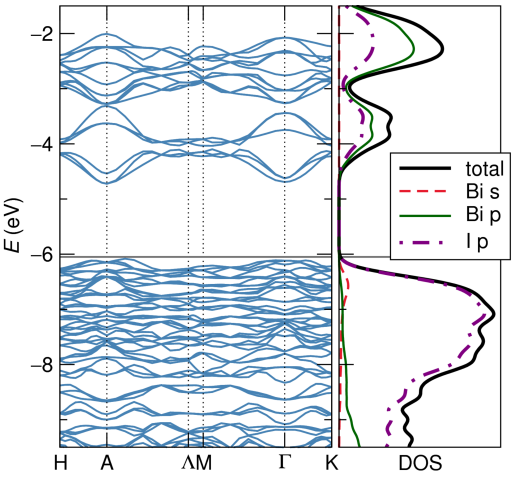

FIG. 3. PBE+SOC band structure of BiI_3 ($R\bar{3}$) between the high symmetry points of the first Brillouin zone of a primitive hexagonal unit cell and HSE+SOC density of states (total DOS scaled). The position of the valence band maximum (VBM, horizontal line) was offset, based on slab calculations.

bulk material) sections of the super-cell used and E_F is the fermi energy of the single unit cell. The results are displayed in Figure 2 together with the BiI_3 crystal structure. As has been established in prior work,[24] Φ_{el} is rather insensitive to the exchange-correlation functional (PBE versus HSE) used as long as SOC is incorporated; thus the time-efficient PBE+SOC scheme was applied. It yields an excellent agreement with the experimental VBM and CBM (VBM+E_g = CBM) determination (Table I). The band structure and the density of states, where the VBM was set to $-I$, are displayed in Figure 3. From the HSE+SOC calculations, the lowest energy tran-

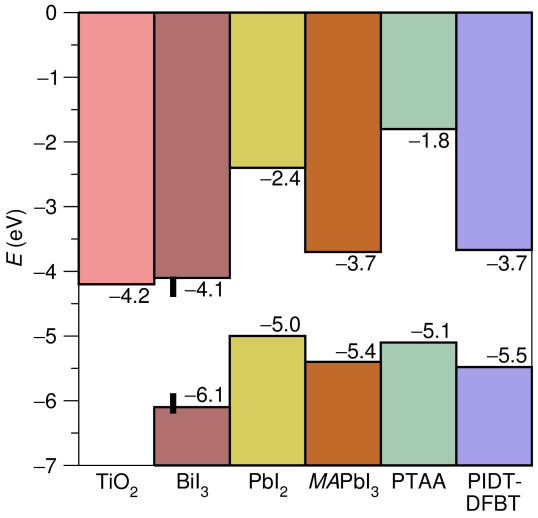

FIG. 4. Band positions derived from DFT calculations (PBE+SOC) carried out on slab models for anatase TiO_2,[24] BiI_3 (this work) and 2H-PbI_2,[24] compared to experimental values for BiI_3 (indicated by vertical bars as a range, for the UPS experiments carried out here). For added comparison, the experimental band positions of $MAPbI_3$[32] (MA = CH_3NH_3), PTAA,[33] and PIDT-DFBT[34] are also displayed.

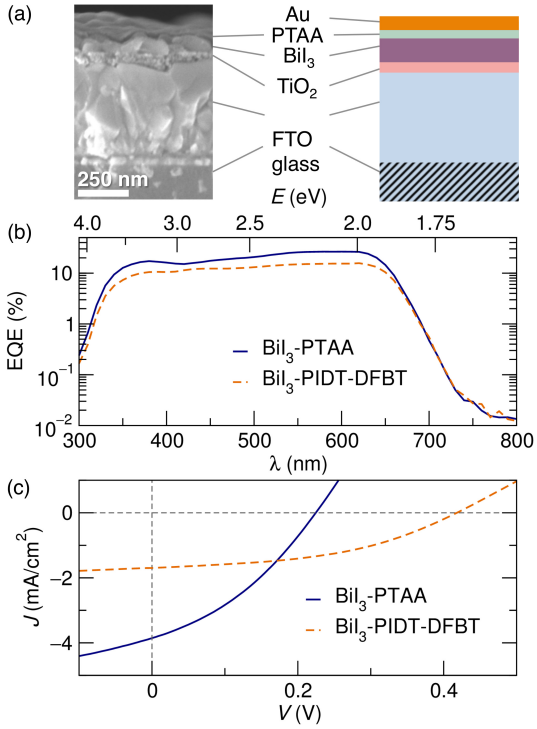

FIG. 5. BiI_3 solar cell devices using PTAA or PIDT-DFBT as the HTL. (a) SEM cross section and schematic device architecture, (b) external quantum efficiency and (c) JV traces of the assembled devices.

sition is indirect (E_g 1.93 eV) between a point at approximately $0.5\overline{A\Lambda}$ in the valence band (VB) and near A (energetically just marginally lower than Γ) in the conduction band (CB). However, the VB band dispersion is so small that the direct excitation requires only marginally more energy. The band dispersion of the CB is more pronounced suggesting a smaller effective mass of electrons compared to holes in BiI_3. Correspondingly, the mobility of electrons has been reported to be 30 times higher than for holes.[29]

While the room-temperature structure of BiI_3 exhibits no signs of a stereo-active Bi^{3+} 6s lone pair, it is inherently apt to undergo lone-pair-induced (ferroelectric) structural distortions.[21] The Born effective charge tensors (Z^*) have been used previously to probe such incipient structural instabilities.[30] The calculated Z^* tensors on Bi^{3+} for BiI_3 of 4.9 to 6.6 (Table I) are significantly elevated compared to the nominal charge, which could be due to a substantial covalent interaction between Bi 6p and halogen p states.[22] Large static dielectric constants and Born charges were suggested to indicate effective screening of defects and impurities which would otherwise trap charge carriers.[31] Therefore we propose that the relatively high Z^* of BiI_3 reported here and previously[21,22] may be correlated with favorable transport properties.

The computational and experimental data on BiI_3 provide a means to determine the materials requirements for appropriate interfacial layers in solar cells. The results of the experimental and computational absolute band determination of BiI_3 are shown in comparison with the related binary PbI_2 (2H-polytype) and the prominent solar cell absorber material $CH_3NH_3PbI_3$ in Figure 4. The CBM of the electron transport layer (ETL), anatase TiO_2, and VBM of the HTL, PTAA, were included because they are commonly used contact materials in solution-processed solar cells.[11] As a fortuitous match, the VBM and CBM of the hybrid perovskite $CH_3NH_3PbI_3$ happen to be very well aligned with the displayed ETL and HTL energy levels allowing for an efficient transfer of both electrons and holes away from the absorber material. For BiI_3 however, while the CBM is well aligned with the TiO_2 CBM for efficient electron injection, the VBM is too far below the VBM of PTAA, PIDT-DFBT, and other common hole transport materials, potentially limiting of the open circuit voltage and thus power conversion efficiency (PCE).

To evaluate the potential of bismuth halides for photovoltaic application experimentally, solar cells with BiI_3 absorber layers were fabricated in a planar heterojunction structure (Figure 5a). Thin films were deposited onto fluorine-doped tin oxide (FTO) on glass under ambient conditions resulting in the final device structure glass/FTO/d-TiO_2/BiI_3/HTL/Au, with the HTL being either the poly-triarylamine PTAA[35] or the poly-indacenodithiophene-difluorobenzothiadiazole PIDT-DFBT[34] (for details see supplemental material[26]), and approximately 100 nm thick BiI_3 layers. Upon illumination, charge carriers can be generated within the BiI_3 layer and at the heterointerface with the ETL TiO_2. The photogenerated electrons are extracted through the

TABLE II. Photovoltaic properties of BiI_3-polymer devices: open circuit voltage V_{oc}, short circuit current J_{sc} (from JV or EQE measurements, respectively), fill factor FF, power conversion efficiency PCE.

Device	V_{oc} (V)	J_{sc} (mA/cm^2)		FF	PCE
		from JV	from EQE	(%)	(%)
BiI_3-PTAA	0.22	3.85	3.79	35	0.30
BiI_3-PIDT-DFBT	0.42	1.70	2.39	45	0.32

TiO_2 layer and the holes are extracted through the organic layer.

The heterojunction solar cells studied here display sub-1 % efficiency, but demonstrate that BiI_3 can be used as the active layer in solution-processed solar cells. Representative external quantum efficiency (EQE) spectra and current density-voltage (JV) characteristics of the solar cell devices are presented in Figure 5b,c and device parameters are summarized in Table II. The EQE spectra of the devices cover the visible spectrum with a sharp absorption onset around 700 nm, which is in good agreement with the BiI_3 optical band gap close to 1.8 eV. It is interesting to note that the low-energy Urbach tail of the EQE of BiI_3 is steep and does not show much structure, potentially suggesting little disorder-induced broadening.[36] The open circuit voltage (V_{oc}) was low as was expected due to the alignment of the transport levels of BiI_3 with the ETL and the HTL (Figure 4). When the deeper VBM polymer PIDT-DFBT is used as the HTL instead of PTAA in the BiI_3 devices, both V_{oc} and FF were improved although a decrease in the J_{sc} was observed. The relatively good quantum efficiency (20% in the PTAA devices) suggests that absorption across the spectrum and charge generation are relatively efficient and therefore improvement of the contacts is likely the best strategy for increasing the PCE of BiI_3 devices.

In summary, working planar heterojunction solar cells using BiI_3 as the light absorber have been presented (PCE 0.32%). The first generation devices exhibit promising quantum efficiencies (EQE 20% in devices with PTAA). The absolute band positions of BiI_3 have been determined both experimentally by UV-Vis and photoemission spectroscopy and computationally by DFT slab calculations with excellent agreement. The relatively low PCE and open circuit voltages of 0.42 V arise from the poor match of the low lying VBM of BiI_3 relative to the VBM of the hole transport layers used. Carrier transfer between active layers could be improved by using HTLs with deeper VBMs.

This work was supported by the U.S. Department of Energy, Office of Science, Basic Energy Sciences under award number DE-SC-0012541. We thank Prof. Jakoah Brgoch for fruitful discussions. A.J.L gratefully acknowledges support of Swiss National Science Foundation fellowship number PBSKP2-145825. The research involved the use of shared experimental facilities of the Materials Research Laboratory and the Center for Scientific Computing at UCSB supported by the MRSEC Program of the National Science Foundation under Award No. DMR 1121053 and NSF CNS-0960316.

[1] A. K. Geim and I. V. Grigorieva, Nature **499**, 419 (2013).
[2] D. B. Mitzi, J. Mater. Chem. **14**, 2355 (2004).
[3] D. Nason and L. Keller, J. Cryst. Growth **156**, 221 (1995).
[4] A. T. Lintereur, W. Qiu, J. C. Nino, and J. Baciak, Nucl. Instrum. Methods Phys. Res., Sect. A **652**, 166 (2011).
[5] H. Han, M. Hong, S. S. Gokhale, S. B. Sinnott, K. Jordan, J. E. Baciak, and J. C. Nino, J. Phys. Chem. C **118**, 3244 (2014).
[6] S. S. Gokhale, H. Han, J. E. Baciak, J. C. Nino, and K. A. Jordan, Radiat. Meas. **74**, 47 (2015).
[7] A. Cuña, I. Aguiar, A. Gancharov, M. Pérez, and L. Fornaro, Crys. Res. Technol. **39**, 899 (2004).
[8] A. Cuña, A. Noguera, E. Saucedo, and L. Fornaro, Crys. Res. Technol. **39**, 912 (2004).
[9] I. Aguiar, S. Kröger, and L. Fornaro, Nucl. Instrum. Methods Phys. Res., Sect. A **610**, 332 (2009).
[10] K. M. Boopathi, S. Raman, R. Mohanraman, F.-C. Chou, Y.-Y. Chen, C.-H. Lee, F.-C. Chang, and C.-W. Chu, Sol. Energy Mater. Sol. Cells **121**, 35 (2014).
[11] N.-G. Park, Mater. Today (Oxford, U. K.) **18**, 65 (2015).
[12] R. E. Brandt, V. Stevanović, D. S. Ginley, T. Buonassi, MRS Commun. **5**, 265 (2015).
[13] M. Ruck, Z. Kristallogr. **210**, 650 (1995).
[14] B. L. Evans, Proc. R. Soc. London, Ser. A **289**, 275 (1966).
[15] Y. Kaifu and T. Komatsu, J. Phys. Soc. Jpn. **40**, 1377 (1976).
[16] S. Kowalczyk, L. Ley, F. McFeely, and D. Shirley, Solid State Commun. **17**, 463 (1975).
[17] I. D. Turjanica, J. Horák, V. M. Benca, and D. V. Čepur, Czech. J. Phys. **18**, 106 (1968).
[18] G. Margaritondo, J. Rowe, M. Schlüter, G. Wertheim, F. Levy, and E. Mooser, Phys. Rev. B **16**, 2934 (1977).
[19] G. Jellison, J. Ramey, and L. Boatner, Phys. Rev. B **59**, 9718 (1999).
[20] N. J. Podraza, W. Qiu, B. B. Hinojosa, H. Xu, M. A. Motyka, S. R. Phillpot, J. E. Baciak, S. Trolier-Mckinstry, and J. C. Nino, J. Appl. Phys. **114**, 033110 (2013).
[21] T. R. Devidas, N. V. Chandra Shekar, C. S. Sundar, P. Chithaiah, Y. A. Sorb, V. S. Bhadram, N. Chandrabhas, K. Pal, U. V. Waghmare, and C. N. R. Rao, J. Phys.: Condens. Matter **26**, 275502 (2014).
[22] D. J. Singh, Phys. Rev. B **82**, 155145 (2010), 1008.2175.
[23] C. G. Van de Walle and R. M. Martin, Phys. Rev. B **34**, 5621 (1986).
[24] J. Brgoch, A. J. Lehner, M. Chabinyc, and R. Seshadri, J. Phys. Chem. C **118**, 27721 (2014).
[25] J. Heyd, G. E. Scuseria, and M. Ernzerhof, J. Chem. Phys. **118**, 8207 (2003).
[26] See supplemental material at [URL will be inserted by AIP] for details of spectroscopy experiments, DFT calculations, and device fabrication.
[27] G. Kresse and J. Furthmüller, Phys. Rev. B **54**, 11169 (1996).
[28] G. Kresse and D. Joubert, Phys. Rev. B **59**, 1758 (1999).
[29] A. Owens and A. Peacock, Nucl. Instrum. Methods Phys. Res., Sect. A **531**, 18 (2004).
[30] M. Miao, J. Brgoch, A. Krishnapriyan, A. Goldman, J. A. Kurzman, and R. Seshadri, Inorg. Chem. **52**, 8183 (2013).
[31] M.-H. Du and D. J. Singh, Phys. Rev. B **81**, 144114 (2010).
[32] P. Schulz, E. Edri, S. Kirmayer, G. Hodes, D. Cahen, and A. Kahn, Energy Environ. Sci. , 1377 (2014).
[33] S. Schols, *Device architecture and Materials for Organic Light-emitting Devices: Targeting High Current Densities and Control of the Triplet Concentration* (Springer Science & Business Media, 2011).
[34] Y. Zhang, S.-C. Chien, K.-S. Chen, H.-L. Yip, Y. Sun, J. A. Davies, F.-C. Chen, and A. K.-Y. Jen, Chem. Comm. **47**, 11026 (2011).
[35] J. Veres, S. Ogier, S. Leeming, B. Brown, and D. Cupertino, Mater. Res. Soc. Symp. Proc. **708**, 1 (2001).
[36] S. De Wolf, J. Holovsky, S.-J. Moon, P. Löper, B. Niesen, M. Ledinsky, F.-J. Haug, J.-H. Yum, and C. Ballif, J. Phys. Chem. Lett. **5**, 1035 (2014).

Supplemental Information:
Electronic structure and photovoltaic application of BiI_3

A. J. Lehner,[1,2] H. Wang,[1] D. H. Fabini,[2,3] C. D. Liman,[1,3] C.-A. Hébert,[2] E. E. Perry,[1,3] M. Wang,[1,4] G. C. Bazan,[1,3,4] M. L. Chabinyc,[1,3] and R. Seshadri[1,2,3,4]

1) *Mitsubishi Chemical Center for Advanced Materials, University of California, Santa Barbara, CA, 93106*

2) *Materials Research Laboratory, University of California, Santa Barbara, CA 93106*

3) *Materials Department, University of California, Santa Barbara, CA 93106*

4) *Department of Chemistry and Biochemistry, University of California, Santa Barbara, CA 93106*

Microscopic and spectroscopic characterization

BiI_3 was used as supplied (Strem 99.999%). Scanning electron microscopy (SEM) images of thin film samples sputtered with gold/palladium to limit charging were collected using a FEI XL40 Sirion FEG digital scanning microscope in backscattered electron imaging mode. Optical spectra in the UV-Vis range from 220 to 800 nm were recorded using a Shimadzu UV3600 spectrometer either in transmission on thin films on quartz glass slides or in diffuse reflection on powder samples which were spread thinly onto compacted $BaSO_4$ powder. Diffuse reflection data was converted using the Kubelka-Munk transformation implemented in the spectrometer's software. Band gaps were extracted from Tauc plots[1,2] of the transmission or Kubelka-Munk transformed reflection data assuming an indirect band gap. A Kratos Axis Ultra XPS/UPS instrument was used for X-ray and ultraviolet photoelectron spectroscopy (XPS and UPS). Samples were prepared by dropcasting or spin-coating from N,N-dimethylformamide solutions as thin films on 10×10 mm pieces of silicon wafers onto which 20 nm of chromium and 90 nm of gold had been deposited by thermal evaporation under high vacuum (10^{-7} torr). Material was removed from one edge of each sample via swabbing with chlorobenzene to expose the gold layer. Nickel tape was used to electrically connect the exposed gold on the top of the substrates to the airtight sample holder which was loaded in a glove box (N_2, $\leq$1 ppm O_2). For XPS, a monochromated Al-Kα source (180 W) was used under ultrahigh vacuum conditions (10^{-8} torr). Survey scans were collected with a step size of 500 meV, a pass energy of 160 eV, and a dwell time of 150 ms. For UPS, a helium I radiation source was used with a gate bias voltage of -9 V. Photoelectrons at the 0° takeoff angle were collected at 600 W (6 kV, 10 mA) with a pass energy of 5 eV and a step size of 25 meV. Survey scans were collected once with a dwell time of 150 ms. Detailed scans near the valence band maximum (VBM) were collected with a dwell time of 600 ms and were repeated 3 times. The position of the VBM was determined from UPS spectra as the energy increment between the left and right edges of the spectral feature, subtracted from the incident photon energy (21.22 eV). We have chosen to determine the spectral width by finding the interception of linear fits to the onset edge as well as the baseline on the low binding energy side. XPS spectra were recorded for every sample before UPS measurements in order to confirm the surface composition (see Figure S1).

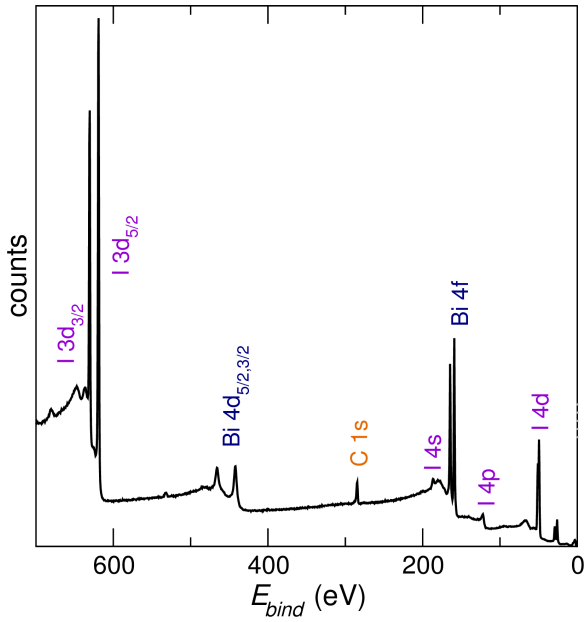

FIG. S1. Example XPS spectrum of BiI_3. For this sample, the surface composition was determined to $BiI_{2.74}$ which is in good agreement with the expected formula within the error of the method.

Details of the density functional theory (DFT) calculations

The DFT calculations of the band structures, band gaps, and absolute band positions were carried out using the VASP Package,[3,4] which implements the Kohn-Sham formulation of the DFT using a plane wave basis and the projector-augmented wave formalism (PAW)[5,6] The input structure for BiI_3 was taken from the literature($R\bar{3}$)[7] without any structure optimization. The energy cut-off of the plane wave basis set was 500 eV. We chose to not include explicit computational treatment of the van der Waals interactions as all the dispersion in the electronic structure is in the direction reciprocal to the in-plane direction and the van der Waals gap does not impact the band offsets. A Gamma center k-mesh grid with a minimum of 20 k-points was employed with the convergence criteria set at 0.001 meV. Absolute band positions were obtained for BiI_3 by constructing slab models using a half-filled $1 \times 1 \times 4$ supercell with two complete unit cells and four additional vacuum (empty) unit cells.[8] Those slab calculations were conducted using the PBE functional[9] including spin-orbit coupling (SOC), which is critical in 6s systems. After reaching the convergence criteria of 0.1 meV, absolute band positions were determined using the macroscopic averaging technique of Baldereschi and coworkers.[10] Accurate band structure and density of states (DOS) calculations were conducted employing the screened hybrid func-

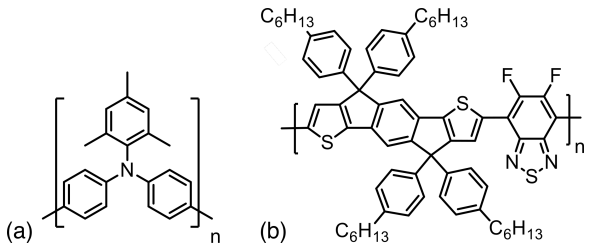

FIG. S2. Hole transport layer materials (a) PTAA and (b) PIDT-DFBT.

tional (HSE06).[11,12] This set of methods was selected based on our previous evaluation of computational schemes for electronic structure and absolute band position calculations for heavy metal main group halides.[13] Born effective charge tensors (Z^*_{ij}) and the static high-frequency (ion-clamped) dielectric tensors (ϵ^{∞}_{ij}) were calculated using a PBE+SOC scheme as reported previously.[13] The crystal structure was visualized using the software VESTA.[14]

Solar cell device fabrication procedure

Step 1) Pre-cut fluorine-doped tin oxide (FTO) coated glasses (1.5 cm$\times$1.5cm, 15 Ω/sq.; Thin Film Devices) were sequentially sonicated in deionized water, acetone and isopropyl alcohol for 10 min each. The substrates were then dried and exposed to UV-ozone for 10 min before use.

Step 2) A dense layer of TiO_2 was deposited on FTO substrates by spin-coating (2000 rpm for 30 s) a solution prepared by dropping 0.035 mL 2M HCl in 2.53 mL ethanol slowly into a solution of tetraisopropyl titanate ($Ti(OiPr)_4$, Aldrich, 0.369 mL in 2.53 mL ethanol) and filtering with a 0.45 m filter. After sintering at 500°C for 30 minutes, the film thickness was determined to be approximately 50 nm by scanning electron microscopy.

Step 3) The bismuth iodide films were obtained by spin-coating a tetrahydrofuran solution of BiI_3 (35 mg/mL, 1000 rpm for 30 s) with a drop of concentrated HI solution added on the dense titania layer. The film was dried at 100°C for 5 minutes to completely remove the solvent.

Step 4) A solution of the poly-triarylamine PTAA[15] (Aldrich, M_w = 17500 g/mol) in toluene (15 mg/1 mL) or the poly-indacenodithiophene-difluorobenzothiadiazole PIDT-DFBT[16] in chlorobenzene (12 mg/1 mL) with 0.0136 mL lithium bis(trifluoromethane) sulfonimide (Li-TFSI) in acetonitrile (Aldrich, 28.3 mg/1 mL) was spin-coated (2000 rpm for 30 s) on

top of the BiI_3 layer as the hole transport layer (see Figure S2).

Step 5) Gold back electrodes were evaporated with a film thickness of 80 nm to complete the device fabrication. The device area was 0.06 cm^2.

The JV characteristics were measured at 1 sun illumination (AM 1.5G, 100 mW/cm^2) in a N_2-filled glovebox with a solar simulator equipped with a Xenon lamp (Newport), a Keithley 2602 Source Meter and a Si reference cell with NIST-traceable calibration. The power conversion efficiency (PCE) was calculated by the following equation: PCE(%) $= 100 \times (V_{oc}) \times (J_{sc})(\mathrm{FF}/P_{inc})$ from the open circuit voltage V_{oc}, the short circuit current J_{sc}, the fill factor FF, and the incident power P_{inc}. The external quantum efficiencies (EQE) were analyzed using a fully computerized measurement system consisting of a 300-W xenon lamp (Newport), a monochromator (Newport CS130), a chopper controller (Newport), two current preamplifiers (SRS SR570), and two lock-in amplifiers (SRS SR810). The light was delivered to the device via a bifurcated fused silica fiber bundle and was focused on the sample with a reflective long working distance microscope lens (Newport) with the spot size much smaller than the device area. A small fraction of the light was focused onto a Si photodiode (Newport) to monitor the intensity. The EQE of the devices was determined relative to reference calibrated Si detector (Newport 818-UV).

REFERENCES

[1]J. Tauc, R. Grigorovici, and A. Vancu, Phys. Stat. Sol. **15**, 627 (1966).

[2]J. Tauc, Mater. Res. Bull. **3**, 37 (1968).

[3]G. Kresse and J. Furthmüller, Comput. Mat. Sci. **6**, 15 (1996).

[4]G. Kresse and J. Furthmüller, Phys. Rev. B **54**, 11169 (1996).

[5]P. E. Blöchl, Phys. Rev. B **50**, 17953 (1994).

[6]G. Kresse and D. Joubert, Phys. Rev. B **59**, 1758 (1999).

[7]M. Ruck, Z. Kristallogr. **210**, 650 (1995).

[8]C. G. Van de Walle and R. M. Martin, Phys. Rev. B **34**, 5621 (1986).

[9]J. P. Perdew, K. Burke, and M. Ernzerhof, Phys. Rev. Lett. **77**, 3865 (1996).

[10]A. Baldereschi, S. Baroni, and R. Resta, Phys. Rev. Lett. **61**, 734 (1988).

[11]J. Heyd, G. E. Scuseria, and M. Ernzerhof, J. Chem. Phys. **118**, 8207 (2003).

[12]J. Heyd, G. E. Scuseria, and M. Ernzerhof, J. Chem. Phys. **124**, 219906 (2006).

[13]J. Brgoch, A. J. Lehner, M. Chabinyc, and R. Seshadri, J. Phys. Chem. C **118**, 27721 (2014).

[14]K. Momma and F. Izumi, J. Appl. Crystallogr. **44**, 1272 (2011).

[15]J. Veres, S. Ogier, S. Leeming, B. Brown, and D. Cupertino, Mater. Res. Soc. Symp. Proc. **708**, 1 (2001).

[16]Y. Zhang, S.-C. Chien, K.-S. Chen, H.-L. Yip, Y. Sun, J. A. Davies, F.-C. Chen, and A. K.-Y. Jen, Chem. Comm. **47**, 11026 (2011).